Achim Wixforth · Christoph Strobl · Ch. Gauer
A. Toegl · J. Scriba · Z. v. Guttenberg

Acoustic manipulation of small droplets

Abstract Surface acoustic waves are used to actuate and process smallest amounts of fluids on the planar surface of a piezoelectric chip. Chemical modification of the chip surface is employed to create virtual wells and tubes to confine the liquids. Lithographically modulated wetting properties of the surface define a fluidic network, in analogy to the wiring of an electronic circuit. Acoustic radiation pressure exerted by the surface wave leads to internal streaming in the fluid and eventually to actuation of small droplets along predetermined trajectories. This way, in analogy to microelectronic circuitry, programmable biochips for a variety of assays on a chip have been realized.

Keywords Biochip · Surface acoustic waves · Droplet · Microarray · Hybridization · PCR

Introduction

Knowledge of the biochemical interior of living cells steadily increases and researchers dig deeper and deeper into the biomolecular world. Now the human genome is sequenced, scientists hope to find novel drug targets once the code is cracked. Analytical techniques like gene expression analysis or cell assays have become standard tools, used in large scale screening for new drugs. The very same technologies are the driving force behind miniaturization of laboratories, as parallel screening requires the smallest amounts of sample for single experiments. The resources of many of the precious ingredients are either very limited or prohibitively expensive.

A. Wixforth (✉) · C. Strobl
Experimentalphysik I, University of Augsburg,
86159 Augsburg, Germany

Ch. Gauer · A. Toegl · J. Scriba · Z. v. Guttenberg
Advalytix AG, Eugen-Sänger-Ring 4,
85649 Brunnthal, Germany

In this article, we wish to report a novel way of tackling the need to scale chemical and biological laboratories down to the size of a thumbnail. We describe a technique which uses virtual beakers and channels to confine smallest amounts of liquids to the planar surface of a microchip, and tiny earthquakes (surface acoustic waves, SAW) on this very chip to act as electrically addressable and programmable nanopumps. The combination of both can be viewed as a step towards the realization of a programmable microfluidic processor.

Materials

1. $LiNbO_3$ piezoelectric substrates for SAW devices
2. High purity metallization (Gold, NiCr, Ti)
3. Silanization surface chemistry (OTS)
4. Kidney and liver tissue of adult female Wistar–Han rats (Charles River Laboratories, Sulzfeld, Germany)
5. RNeasy Maxi Kit incl. on-column DNase digestion (Qiagen, Hilden, Germany)
6. Label Star Array Kit (Qiagen)
7. Cyanine-3-dCTP for rat kidney (Perkin Elmer Life Sciences, Freiburg, Germany)
8. Cyanine-5-dCTP for rat liver cDNA
9. ArrayDesigner 2 (Premierbiosoft, Palo Alto, CA, USA)
10. Epoxy coated glass slide (Advalytix, Brunnthal, Germany)
11. Gene Machines OmniGrid contact printer
12. SMP3 split pin (Telechem, Sunnyvale, CA, USA)
13. 0,2% (w/v) SDS
14. DD H_2O
15. 4X SSC/0,1% (*w*/*v*) Sodium dodecyl sulfate (SDS)/ 1% (*w*/*v*) bovine serum albumin (Sigma)
16. ArrayBooster Hybridization station (Advalytix, Brunnthal, Germany)
17. AdvaCard micro mixer card (Advalytix)
18. AdvaHyb Hybridization Buffer (Advalytix)
19. 22×22-mm cover glasses (Sigma)
20. Fixogum glue (Marabu, Tamm, Germany)

21. GenePix4000B Scanner (Axon Instruments, Union City, CA, USA)
22. GenePix Pro 4.0 Software (Axon Instruments)
23. QIAquick PCR Purification Kit (Qiagen)

Methods

Surface acoustic waves

Surface acoustic waves were first described in combination with earthquakes [1]. Meanwhile, reduced to the significantly smaller nano scale, they found their way into much friendlier fields: SAW devices are widely used for RF signal processing and filter applications and have become a huge industry in mobile communication [2]. SAW devices have been around for years in communication circuitry—every cellphone has filters using the effect. An electrical signal fed into so-called transducers on the surface of a piezoelectric chip is converted into a deformation of the crystal underneath. Given the right frequency of the signal, a mechanical wave is launched across the chip. In Fig. 1, we sketch a snapshot of a SAW propagating on a solid.

The SAW in this figure is characterized by alternating regions of compressed and expanded material as indicated in gray scale.

In the recent past, SAW have also been used to act in a completely different way than for filtering and signal processing just by converting electrical signals into mechanical vibrations and vice versa. Excited on piezoelectric substrates, they are accompanied by large electric fields. These electric fields travel at the speed of sound for the substrate (approximately 3,000 m s^{-1}) having the same spatial and temporal periodicity as their mechanical companions. Charges at or close to the surface couple with these electric fields, and currents are induced within a conducting layer. Nearly 20 years ago, we thus introduced SAW to study the dynamic conductivity $\sigma(\omega,k)$ of low-dimensional electron systems in high magnetic fields and at low temperatures. It turns out that the interaction between a SAW and the mobile charges in a semiconductor is strongest for very low sheet conductivities as they are observed, e.g., in the regime of the quantum Hall effect [3]. However, SAW can not only be used to probe the properties of quantum systems, but also to deliberately alter some of them, because SAW represent a spatially modulated strain and stress field accompanied by strong electric fields in a solid, and propagating at the speed of sound. Such an interaction between SAW and the optical properties of a semiconductor quantum well led us to the discovery that photogenerated electron–hole pairs in a semiconductor quantum well can be spatially separated under the influence of a SAW-mediated electric field. This, in turn has an enormous impact on the photoluminescence (PL) of the semiconductor. We were able to show that not only the PL is quenched under the influence of a SAW, it can also be re-established at a remote location on the sample and after a certain delay time [4]. Further studies include acoustic charge transport and the creation of dynamically induced electron wires, and the study of nonlinear acoustic interaction with low dimensional electron systems in semiconductors [5, 6].

However, the piezoelectric effect is usually only a small contribution to the elastic properties of a solid: most of the energy propagating in a SAW (usually more than 95%) is mechanical in nature. Hence, not only electrical interactions as described above, but also mechanical interactions are a possible scope for experimental investigations. Having wavelengths of a few microns and amplitudes of about only a nanometer, however, the forces and electric fields within the nanoquake are sufficient to have a macroscopic effect. Any piece of matter on the surface in the path of a SAW experiences its vibrating force: viscous materials like liquids absorb much of their energy. It turns out that the interaction between a SAW and a liquid on top of the substrate surface induces internal streaming, and, as we will point out below, at large SAW amplitudes this can even lead to a movement of the liquid as a whole.

Acoustic streaming

The origin of such acoustically induced internal streaming is depicted schematically in Fig. 2. A SAW is propagating from left to right along the x-axis. At $x=0$, it reaches the boundary of a liquid at the surface of the substrate. A SAW with a non-vanishing amplitude in the z-direction, i.e. normal to the surface of the substrate, is then strongly absorbed by the fluid, as indicated by the

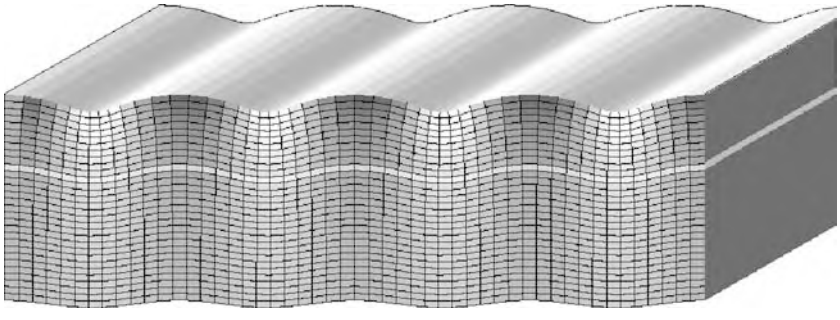

Fig. 1 Sketch of a SAW propagating on a piezoelectric substrate. Typical wavelengths are in the micrometer range, typical amplitudes less than a nanometer

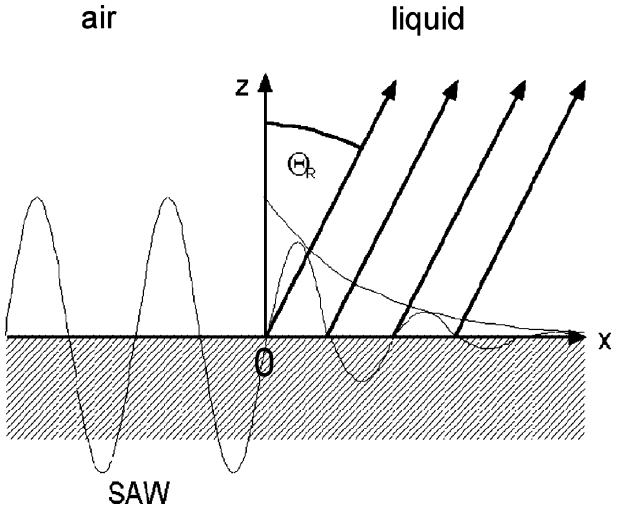

Fig. 2 Schematic illustration of the interaction between a SAW and a liquid on the surface of the SAW substrate. The SAW is propagating from left to right, and at $x=0$ hits the liquid. A longitudinal sound wave is radiated into the fluid under a refraction angle Θ_R

decaying amplitude for positive x values. Moreover, it creates a small but finite pressure difference $2\Delta p$ in the fluid between the ridges and the wells of the wave, which transforms into a small but finite difference $2\Delta\rho$ in the liquid density. Both quantities then spatially and temporally oscillate around their respective equilibrium value p_0, and ρ_o, respectively. The pressure difference directly above the surface of the substrate leads to the excitation of a longitudinal sound wave into the liquid. As the sound velocities for the liquid and the solid substrates are in general not equal, this wave is launched under a diffraction angle Θ_R, given by:

$$\Theta_R = \arcsin\left(\frac{v_S}{v_f}\right)$$

Here, v_s and v_f denote the sound velocities of the substrate, and the fluid, respectively. In addition, the SAW is responsible for the build-up of an acoustic radiation pressure [7]

$$P_S = \rho_0 v_S^2 \left(\frac{\Delta\rho}{\rho_0}\right)^2$$

in the direction of the sound propagation in the fluid. This leads to internal streaming in a closed volume like a droplet, as the boundary of the droplet reflects the actuated fluid back to the source. Such internal SAW-driven streaming in a small droplet can be nicely visualized by dissolving a dried fluorescent dye under the influence of a SAW. In Fig. 3, we depict two snapshots of such a fluorescence experiment, taken approximately 1 s apart from each other.

For larger SAW amplitudes, the acoustic radiation pressure even deforms the droplet surface at the opposite side of the sound entrance. This can be seen in Fig. 4, where we show a droplet under the influence of a quite intense SAW, impinging from the left. As can be seen from the figure, the acoustic radiation pressure in this case is so high that it strongly deforms the droplet. At the same time, the wetting angles to the left and the right of the droplet (i.e. "luff and lee" of the SAW) are modified with respect to the equilibrium values. This acoustically driven deformation of the droplet is the main reason for the droplet actuation in our case.

Virtual containers and tracks for liquids on a chip

The next step towards an application of SAW in microfluidics in general is to create "flatland" [8] analogs to channels, tubes, reservoirs, mixing chambers, and similar building blocks usually employed to guide, contain, or process liquids in a fluidic network.

By chemical modification of parts of the chip surface (e.g. silanization employing an OTS-based surface chemistry) we are able to create patterns of preferred wettability (hydrophilic regions) separated by regions of surface chemistry where fluids are repelled (hydrophobic areas). Employing lithographic techniques borrowed from semiconductor microelectronics we can thus create completely flat, 2D fluidic networks, where liquids are confined to virtual tracks, reservoirs and reaction chambers by surface tension alone. A whole variety of methods is available to modulate the wetting properties of the surface of a chip: the most common technique is to silanize specific areas of the surface whereas other regions of the surface are protected by laterally structured photo resists, that have been exposed, using a mask, to UV radiation and subsequently developed leaving the exposed areas etched through to the chip surface.

In Fig. 5, we depict some such self-assembled virtual potential wells for fluids on a surface. Photolithographic techniques have been employed to create "containers" for extremely small amounts of liquid, with predeter-

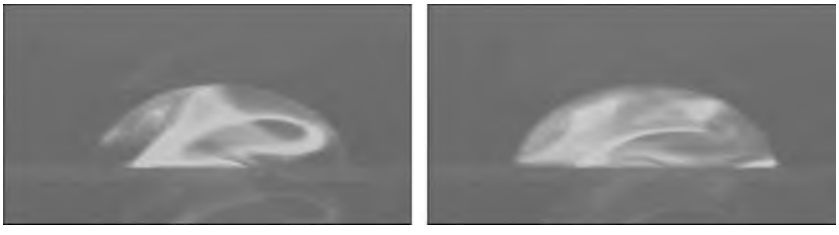

Fig. 3 SAW-induced internal streaming in a small water droplet (side view, approximately 50 nL). A dried fluorescent dye on the surface of the chip is dissolved by SAW agitation, and rapidly fills the whole droplet volume

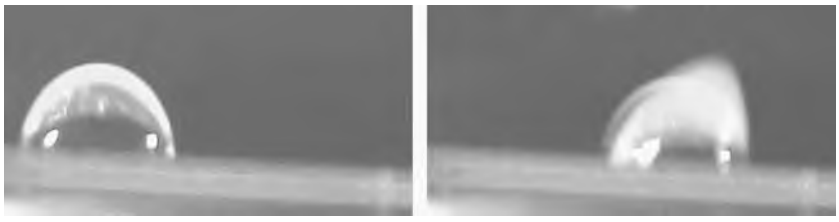

Fig. 4 Side view of a small droplet (ca. 50 nL) on the surface of a piezoelectric substrate. *Left:* Droplet at rest, note the wetting angle of about 90 °, which has been obtained by hydrophobic treatment of the surface. *Right:* droplet being "hit" by a SAW impinging from the left. The acoustic radiation strongly deforms the droplet shape. This leads to momentary asymmetry of the wetting angles of the droplet

mined shapes like a hexagon (left) or a "tube" with a narrowing (which acts, incidentally, as a pressure-driven valve). Given this surface functionalization, either closed fluid volumes or single droplets can be acoustically guided along predetermined pathways along the surface of the chip.

Given such chemically defined virtual tracks and the SAW-based actuation, we can thus move several droplets of different fluids (or generally different reagents) independently in any desired direction. In Fig. 6, we give a series of snapshots of one of our fluidic chips, where three droplets are actuated using SAW agitation. Depending on the actual layout of the chip, the droplets can be split into smaller ones, they can be merged, mixed and processed in almost any fashion. As the SAW nanopumps are electrically addressable, a complete sequence of different steps of a chemical "experiment" or a biological assay can be computer-controlled. Moreover, the simplicity of the fabrication process of our "programmable bioprocessors" makes them a serious candidate for truly miniaturized laboratories on a chip [9].

It turns out that the interaction between a SAW and a droplet on a flat surface of a chip is highly non-linear in terms of the ratio between the SAW wavelength and the droplet diameter. In other words, for a given SAW wavelength and power, only droplets of a certain volume can be effectively actuated along a fluidic track, whereas droplets of smaller volume remain basically unaffected by this acoustic pressure. This effect can be used to create very small droplets (approximately 50 pL) out of a larger one (approximately 50 nL) by leaving them behind on a microstructured chemically modified surface (see Fig. 7). Such an array of ultra small droplets can be regarded as a special form of microarray. For special applications a layer-by-layer build up of complex sandwich systems might also be generated by employing this scheme.

A combination of the non-linear interaction between the SAW and a droplet and a geometrically defined "dispenser" geometry can be used to deliberately "meter" a defined volume from a larger one. This is shown in Fig. 8, where we show a part of a chip, where a larger droplet (approximately 100 nL) is used again as a reservoir to dispense a small droplet. After separation from the reservoir, the small droplet then is moved to another location of the chip for further processing.

Applications

SAW-driven agitation of hybridization assays

First applications of the SAW based fluidic actuation already exist and are presently commercialized: the ability of SAW to efficiently stir and mix extremely small amounts of fluids is employed to enhance the results of biological hybridization assays. During hybridization, immobilized DNA fragments or oligonucleotides which are spotted on a microarray are flooded by an unknown sample fluid containing other oligonucleotides. Once hybridization occurs, fluorescence markers on the sample molecules accumulate at a specific spot. This fluorescent signal can then be detected and act as a measure of the hybridization efficiency, in other words, the degree of matching between sample and target molecule.

Usually, such micro array hybridizations are performed in a thin capillary fluid film (thickness approxi-

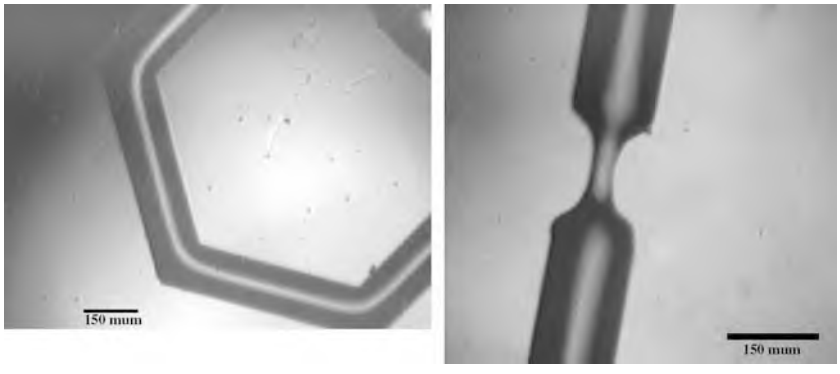

Fig. 5 Photolithographically defined surface modification to modulate its wettability. This way, "virtual" fluidic tracks are created to confine extremely small amounts of liquid to predetermined geometries or to guide a SAW-driven droplet along a predetermined path on the chip surface

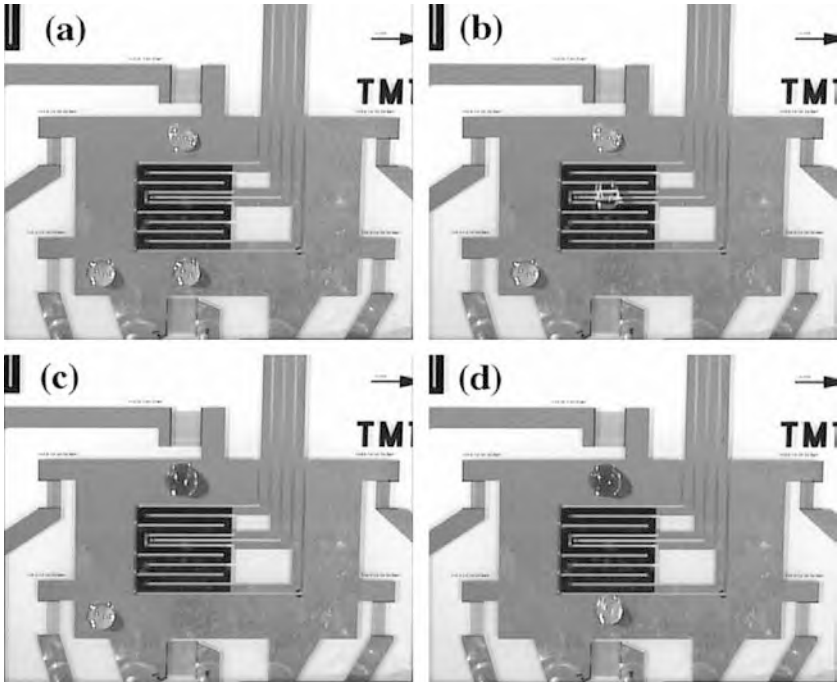

Fig. 6 A SAW driven microfluidic processor. Three droplets (approximately 100 nL each) are moved under "remote control" and independently by the nanopumps. **a**–**d** represent a series of sequentially taken snapshots to visualize the movement, and the "nanochemical reactions" occurring when the droplets are merged and mixed by the action of the surface wave. The chip not only contains the nanopumps and the fluidic environment but, in the centre, additional components such as sensors and heaters

mately 50 μm), spread across the area of a conventional microscope slide (7.5×2.5 cm). Here, the narrowness of the film again leads to a complete suppression of turbulent flow in the film, diffusion is the only driving force to move a sample molecule toward a target spot.

In Table 1, for instance, we have calculated the diffusion time needed to overcome a certain distance in such a thin liquid film. To cover a distance of only 1 mm, a 100 nm long DNA fragment needs already approximately 30 h. This diffusion limit together with the then unavoidable depletion effects leads to a very slow hybridization process for microarrays. Obviously, mixing and stirring the fluid in the narrow slit would improve this process, as the diffusion limit can be overcome in this case. Although even SAW-mediated agitation in a thin liquid film is rather slow as compared to a free fluid surface, the diffusion limit can be definitely overcome, as we show in Fig. 9.

Here, we depict the result of the fluorescence analysis of a typical microarray assay for the diffusion only, and the mixed case. Not only do we observe a quite dramatic increase of the signal intensity in the latter case, also the homogeneity of the single spots on the microarray is much better for the agitated sample [9]. Another important issue that is associated with microagitation of microarray hybridization assays is the fact that by overcoming the diffusion limit, it is now possible to actually monitor the temporal evolution of the hybridization process. This gives the research an additional channel of information to further improve the results of such macro molecular experiments.

Example: hybridization efficiency of polymer chain reaction (PCR)-product vs. oligonucleotide microarrays

Microarrays for gene expression studies fall into two categories with respect to the type of spotted probe molecules: PCR products amplified from cDNA clones or presynthesized oligonucleotides. Both systems have their specific advantages regarding biological function-

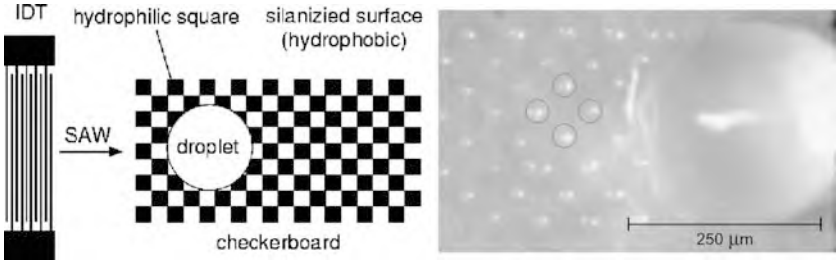

Fig. 7 Loading of a microarray with a spot distance of about 70 μm using an acoustically actuated droplet moving from left to right acting as a reservoir. Within the fluidic track, a checkerboard geometry of specially treated surface areas has been lithographically defined. The large droplet of about 50 nL volume selectively wets these areas, leaving an array of small droplets behind, each having a volume of only 50 pL. The *small circles* have been added to the figure to visualize the contours of the smaller droplets

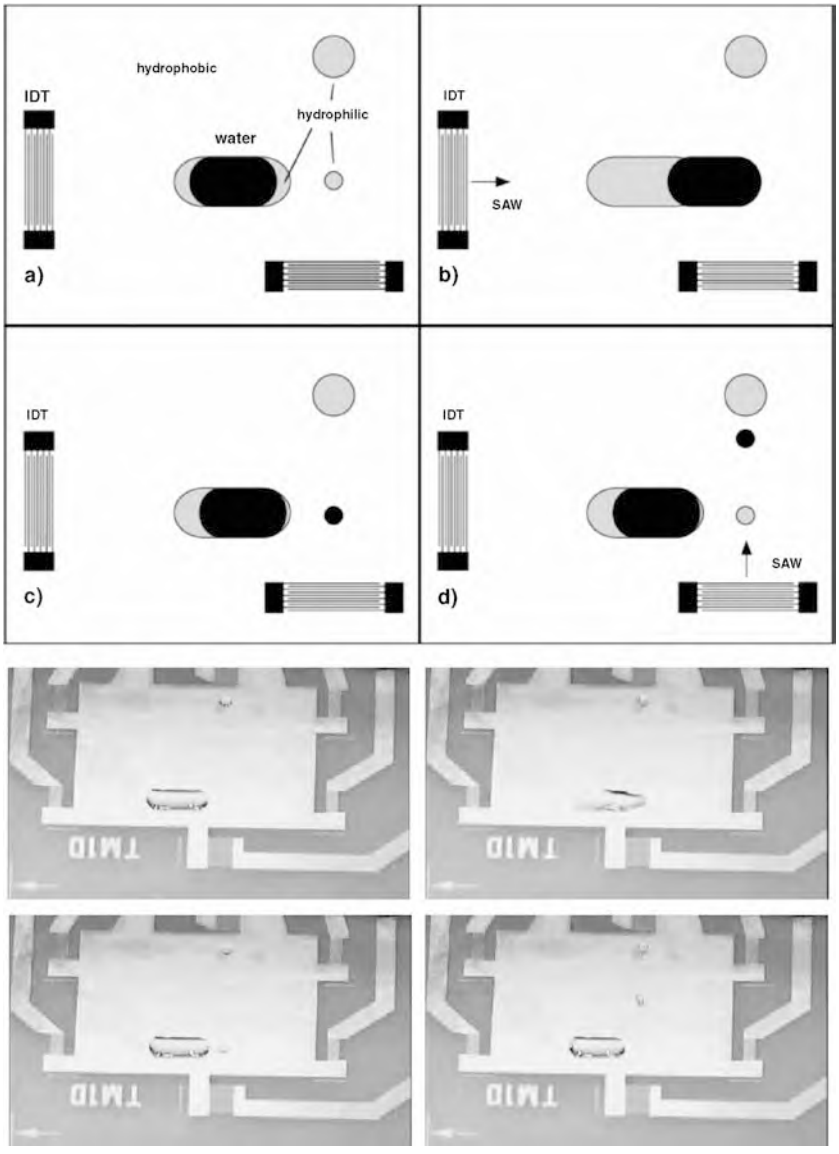

Fig. 8 Acoustically driven nano dispenser by selective chemical modification of the wettability of parts of the chip surface and employing two SAW propagating at a right-angle to each other. The *upper part* shows the timing of the dispensing process, in the *lower part* we depict the actual experiment

ality and cost. In this study, we compared the signal-to-noise ratios of cDNA hybridized simultaneously to spotted PCR products and oligonucleotides [10]. To exclude any variations induced by sample preparation, hybridization, and washing conditions we used hybrid slides, i.e. the PCR products and oligonucleotides were spotted on the same slide.

Ten PCR products were amplified using rat liver genomic DNA as a template and checked for sequence consistency after purification with QIAquick PCR Purification Kit (Qiagen). The PCR products were then spotted in one 10×10 subarray with ten replicate spots in a row. Another 10×10 subarray consists of the corresponding 50-mer (14) oligonucleotides (ten replicates each) specific for the same genes. Each oligonucleotide had been designed to represent a part of the PCR product sequence (mostly at the 5′-end) to ensure comparability between both types of spotted molecule. All probes, oligos and PCR products, were designed with a GC-content of 50%. We used Advalytix epoxy-coated slides for spotting the PCR products and oligonucleotides, again using a contact printing system with Telechem SMP3 split pins.

The spotting concentration for the PCR products was 0.5 pmol μL^{-1}, for the oligonucleotides 50 pmol μL^{-1} in a spotting buffer containing DMSO to ensure that the PCR products are basically single-stranded while binding to the slide surface. The spotting concentrations were optimized separately such that the signal intensities

Table 1 Calculated diffusion times for different diffusion lengths and three different particle sizes. A DNA segment of only 100 nm lengths needs about 30 h to diffuse over a distance of only 1 mm

diffusion length (μm)	potassium ion (0.2 nm)	Oligonucleotide (6 nm)	PCR product (100 nm)
1	0.2 ms	6 ms	100 ms
10	20 ms	600 ms	10 s
100	2 s	60 s	20 min
1000	200 s	100 min	30 h

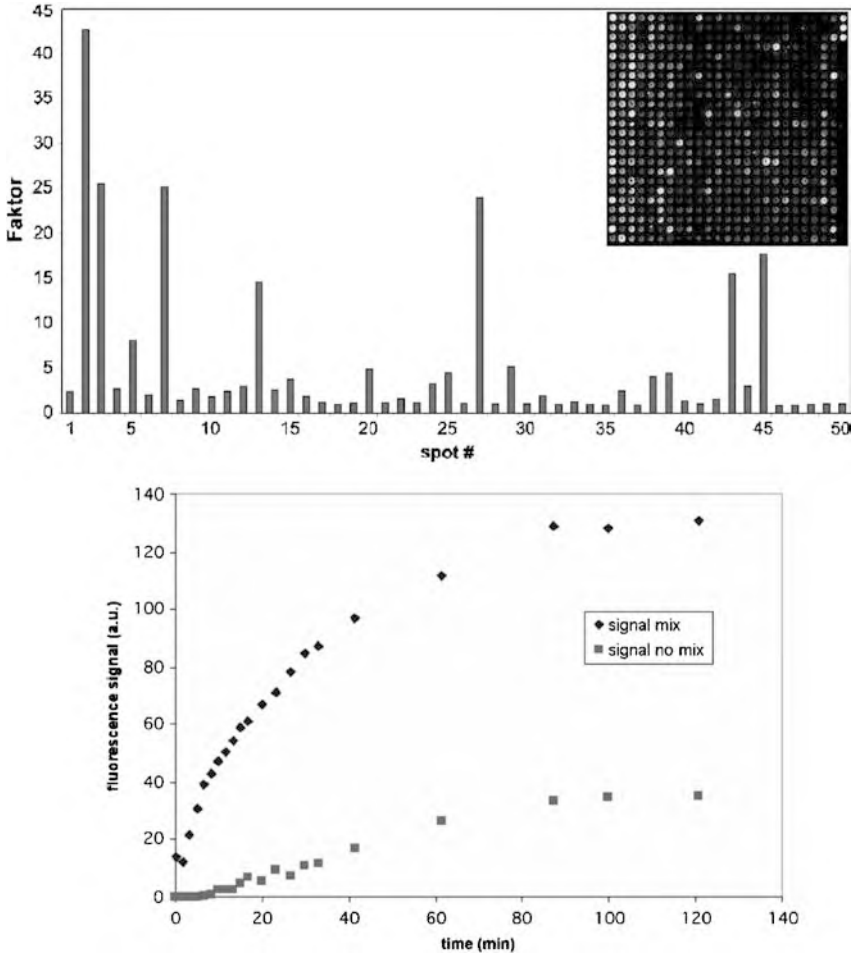

Fig. 9 Result of a fluorescence-labelled micro array experiment (rat chip with 50 oligos, three subarrays, two replicas each, overnight hybridization at 42 °C). In **a** we show the intensity enhancement for different spots on the microarray for the agitated sample fluid as compared to the diffusion limited case. The *inset* shows a typical microarray. In **b** we depict the temporal evolution of the fluorescence intensity in such an experiment

reached their maximum in overnight hybridization. Higher spotting concentrations showed no further effect on the signal intensity. Post spotting processing was carried out according to the slide manufacturer's manual for PCR products including a denaturation step. In Table 2, we show the gene identity and the lengths of the spotted PCR products.

The hybridization was carried out using Cy3 directly labeled cDNA from 5 μg rat liver total RNA using the Qiagen Label Star Array Kit. The slides were pre-hybridized in a 1% BSA, 4xSSC, and 0.5% SDS solution at 42 °C. Stringent washing after overnight hybridization was carried out in 2xSSC/0.1%SDS, 1xSSC and 0.5xSSC for 10 min each. All hybridizations were again done in the *ArrayBooster* with no mixing and with mixing activated (default program ''42 °C DNA-high''). The hybridization volume was 40 μL (*AdvaCard* AC1a) in all cases, i.e. we worked with the same amount and concentration of target molecules by using a pooled aliquot. The only conditions changed were mixing and incubation time. A time series with 8, 20, 32, 48 and 72 h of incubation time was carried out.

Table 2 Gene identity and fragment length of the rat PCR products

No.	Gene	PCR product length
1	af 106860	292
2	x94242	297
3	j02742	143
4	x68282	324
5	m13501	596
6	m18053	155
7	l10339	193
8	x62145	428
9	x66370	337
10	x06483	348

For microarray scanning and image analysis we used again the Gene Pix 4000B scanner and the Gene Pix Pro 4.1 Software (Axon Instruments) for raw data generation. All signal intensities were corrected for the local background. We used the background corrected signal intensity rather than the signal-to-noise ratio as the signals were generally at least one order of magnitude higher than the background. Instruments settings were Laser Power 100% and PMT 600 using the rainbow 2 false colour table for visualization.

In Fig. 10a, we show an image of a static (no agitation) hybridization with a 72 h incubation time. The PCR probes result in a higher signal intensity than their oligonucleotide counterparts. The gain in signal intensity achieved by using PCR products compared to

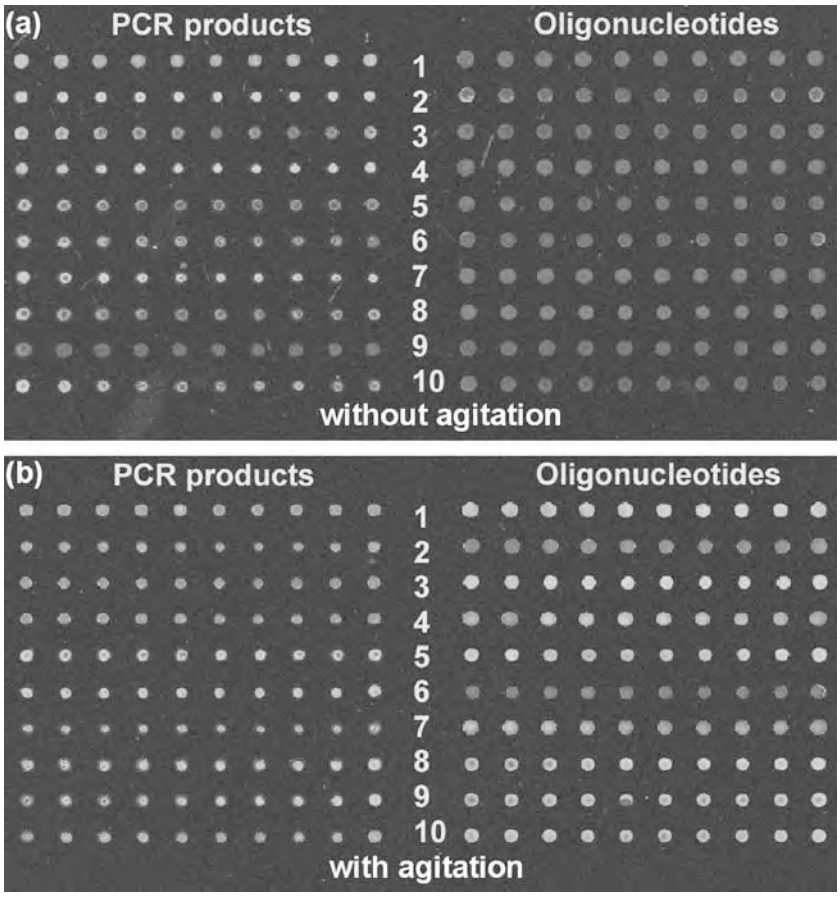

Fig. 10 **a** Static experiment without micro agitation at 42 °C; 72 h hybridization time. **b** Micro agitated hybridization experiment under the same conditions

oligonucleotides varies from 1.1 (row 9) to 10.2 (row 4). The PCR spots are generally smaller than their oligonucleotide counterparts so that this difference may be caused in part by cDNA molecules binding to a larger area.

Active micro agitation of the hybridization solution improved the signal intensities for both oligonucleotides and PCR products, as can be seen in Fig. 10b. However, the average amplification factor differs substantially. The gain in signal intensity was about threefold for PCR products and about 16-fold for oligonucleotides after incubation for 72 h. This pronounced amplification of oligonucleotide signal intensities by micro agitation has been found for all incubation times (Fig. 11). As a result, agitation reversed the relative signal intensities of PCR products and oligonucleotides. With agitation, oligo

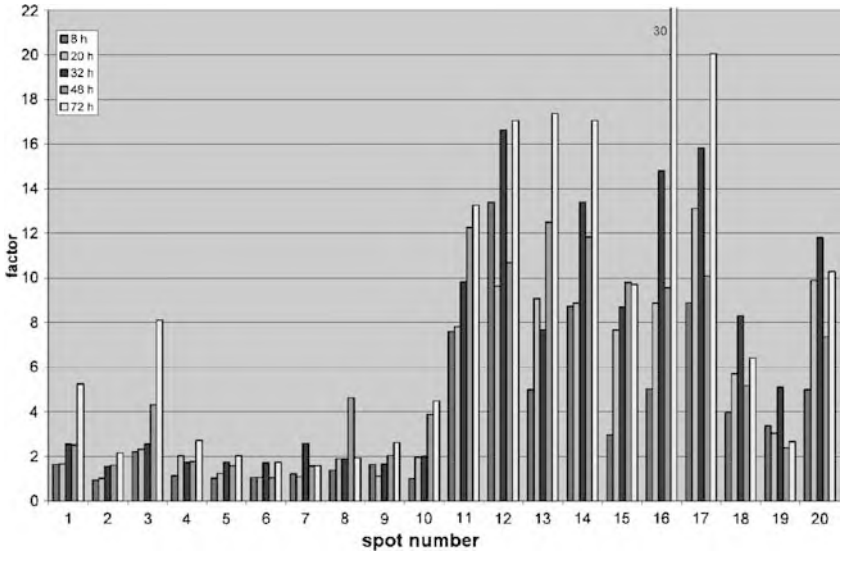

Fig. 11 Amplification factor due to micro agitation on a (PCR product)/(oligonucleotide) hybrid slide at different hybridization times. For all spots and all hybridization times significant amplification of the signal intensities was obtained. However, the amplification factor differs from about 1.1 up to more than 30 for different spots

probes give higher intensities for all experimental conditions investigated, whereas PCR products result in higher signals without agitation. It is worth noting that the 72 h signal intensities are lower than the values at 48 h of incubation. Further studies are under way to corroborate this finding.

Under static hybridization conditions (no agitation) we assume the number of target molecules within the diffusion radius limits the signal intensity for both spot types. In this case, the spotted PCR products exhibit a higher signal intensity as compared to the corresponding oligonucleotides, because their binding constant is larger. With micro agitation the signal intensity is no longer determined by the number of target molecules in the immediate vicinity of the spots. Under these conditions the larger number of binding sites on the oligo spots might over-compensate for the different binding constants. For this specific array we estimate the number of binding sites on the oligonucleotide spots to be at least two orders of magnitude larger than for PCR products. In a separate experiment we found that almost all oligo molecules spotted on the chip act as binding sites. As the concentration of PCR products in the spotting buffer was about two orders of magnitudes lower than for oligonucleotides, we conclude that the number of available binding sites is also lower by the same factor. Furthermore, the renaturation of the PCR product double-strand sections might compete with the hybridization of the target molecules which results in a further reduction of the number of binding sites available.

PCR on a chip

The ability of our novel, acoustically driven, programmable bioprocessors to actuate small liquid droplets, to stir them during hybridization, etc., led us to an attempt to perform a complete PCR on a chip.

For this purpose, in co-operation with the Institute for Physical High Technology (IPHT) in Jena, Germany, we have integrated the fluid-handling techniques described above with a micro heater and a thermometer on the planar surface of the chip. Heating and cooling rates of the order of 5 K s^{-1} have been achieved on this chip (Fig. 12).

As a proof of concept, a standard PCR protocol (genomic DNA with STS primer, main product 150 base pairs) has been scaled down to a droplet size of less than 1 μL. A PCR mix containing polymerase, primer, d-NTP, template DNA, and reaction buffer formed the sample droplet. To prevent this small droplet from evaporation it was covered by a small amount of mineral oil. Thus, the sample droplet and the oil cover formed a virtual micro reactor which could be actuated as a whole across the chip surface. The technological challenge behind this process was to simultaneously define hydrophobic and lipophobic areas and tracks on the chip surface. In the present case (inset of Fig. 12), we achieved a wetting angle of about 80° for oil and water.

Both on-chip microarray detection and a subsequent gel electrophoretic test showed that PCR on a chip is feasible and that after even 30 cycles only three start copies in the droplet could be successfully amplified. As a very attractive addition to this on-chip PCR, we were also able to show that multi spot PCR is also possible. For this purpose, up to four different sample droplets have been covered by oil, simultaneously (Fig. 12, centre). The PCR, too, was performed simultaneously for the four droplets. Subsequent analysis showed no cross-contamination between the single droplets (Fig. 12, lower inset).

A very important feature of the on-chip PCR is that we are able to monitor the progress of the amplifica-

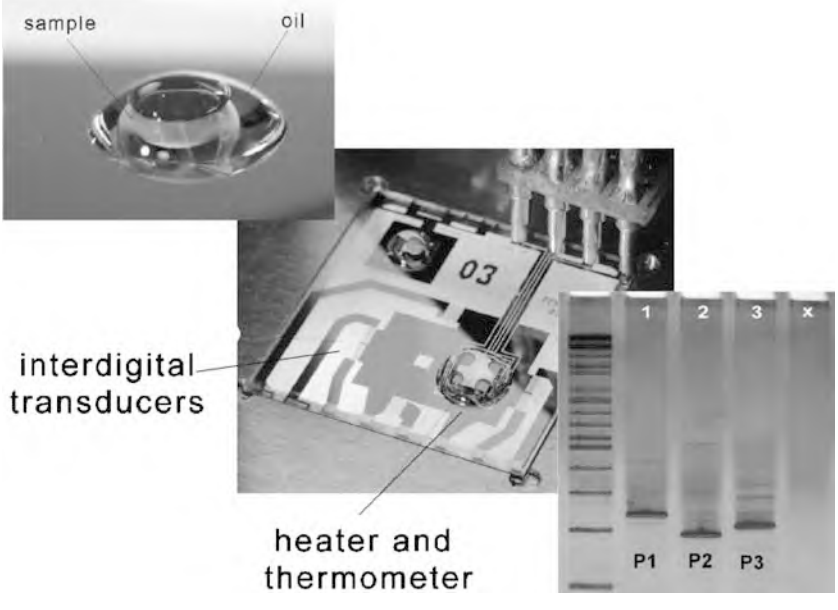

Fig. 12 Chip-based PCR as a proof of concept for a programmable bioprocessor. On the chip (*centre*), interdigital transducers for acoustic manipulation of the small droplets and a heater and a thermometer have been integrated simultaneously. Four different PCR protocols have been performed at the same time, employing a "multi-spot" technique as described in the text. To prevent the small sample droplets (less than a microlitre) from evaporation during the PCR cycles, all four droplets were covered by an oil drop (see also *upper inset*). Subsequent gel electrophoresis showed that no cross contamination between the droplets (samples P1–P3 and a control droplet, lane *X*) occurred

tion in situ—again mediated by SAW-driven agitation which favours the dynamic processes involved.

The on-chip PCR is still under evaluation but we expect to describe the whole process in detail in the near future.

Summary

In summary, we have described a novel and unconventional method for microfluidic fluid handling for very small sample volumes. Surface acoustic waves on a piezoelectric substrate strongly interact with a liquid on the surface of this substrate which leads to build up of acoustic radiation pressure in the fluid. This pressure is basically the origin of SAW-mediated internal streaming in the fluid and of actuation of small droplets as a whole. Laterally patterned surface modification also enables the creation of fluidic tracks, containers, or functional elements for a planar microfluidic network. Programmable actuation of different small droplets together with a wealth of possible fluidic functional blocks is a step toward realization of a programmable fluidic microprocessor.

Acknowledgements This work was sponsored in part by the German Bundesministerium für Bildung und Forschung, BMBF, and in part by the Bayerische Forschungsstiftung under the program "FORNANO". The present work would have been impossible without the support of many of my students and colleagues. I would like to especially thank the crew of Advalytix, Brunnthal for their efforts to make a crazy idea into a product that really works and sells.

References

1. Lord Rayleigh (1985) Proc London Math Soc 17:4
2. Auld BA (1973) Acoustic fields and waves in solids. Wiley, New York
3. Wixforth A, Kotthaus JP, Weimann G (1986) Phys Rev Lett 56:2104
4. Rocke C, Zimmermann S, Wixforth A, Kotthaus JP, Böhm G, Weimann G (1997) Phys Rev Lett 78:4099
5. Rotter M, Kalameisev AV, Govorov AO, Ruile W, Wixforth A (1999) Phys Rev Lett 82:2171
6. Rotter M, Wixforth A, Govorov AO, Ruile W, Bernklau D, Riechert H (1999) Appl Phys Lett 75:965
7. Lord Rayleigh (1905) Phil Mag 10 (Ser 6):364–374
8. Edwin A. Abbott (ed) (1894) Flatland: a romance of many dimensions
9. Wixforth A, Scriba J, Gauer C (2002) mstNews 5/2002:42 (2002).
10. Toegl A, Kirchner R, Gauer C, Wixforth A (2003) J Biomol Tech 14:197–204